

# DLinear-based Prediction of Remaining Useful Life of Lithium-Ion Batteries: Feature Engineering through Explainable Artificial Intelligence

Minsu Kim<sup>a,1</sup>, Jaehyun Oh<sup>b,1</sup>, Sang-Young Lee<sup>b,c,‡</sup>, Junghwan Kim<sup>b,c,z</sup>

<sup>a</sup>Department of Chemical Engineering, Massachusetts Institute of Technology, Cambridge, Massachusetts 02139, United States of America

<sup>b</sup>Department of Chemical and Biomolecular Engineering, Yonsei University, Seoul 03722, Republic of Korea

<sup>c</sup>Department of Battery Engineering, Yonsei University, Seoul 03722, Republic of Korea

January 22, 2025

## Abstract

Accurate prediction of the Remaining Useful Life (RUL) of lithium-ion batteries is essential for ensuring safety, reducing maintenance costs, and optimizing usage. However, predicting RUL is challenging due to the nonlinear characteristics of the degradation caused by complex chemical reactions. Machine learning allows precise predictions by learning the latent functions of degradation relationships based on cycling behavior. This study introduces an accurate RUL prediction approach based on feature engineering and DLinear, applied to the dataset from NASA’s Prognostics Center of Excellence. Among the 20 features generated from current, voltage, temperature, and time provided in this dataset, key features contributing to degradation are selected using Pearson correlation coefficient and Shapley values. Shapley value-based feature selection effectively reflects cell-to-cell variability, showing similar importance rankings across all cells. The DLinear-based RUL prediction using key features efficiently captures the time-series trend, demonstrating significantly better performance compared to Long Short-Term Memory and Transformer models.

**Keywords**— Lithium-Ion Batteries, Remaining Useful Life, Feature Engineering, DLinear, Cell-to-Cell Variability

---

<sup>‡</sup>Corresponding author [syleek@yonsei.ac.kr](mailto:syleek@yonsei.ac.kr).

<sup>z</sup>Corresponding author [kjh24@yonsei.ac.kr](mailto:kjh24@yonsei.ac.kr).

<sup>1</sup>These authors contributed equally to this work.

# 1 Introduction

The Electric Vehicles (EVs) industry has grown rapidly due to environmental issues related to internal combustion engine vehicles. Lithium-Ion Batteries (LIBs) are the most widely used battery materials based on their advantages such as high energy density, low self-discharge characteristics, and long lifespan [1]. However, it is inevitable that battery performance will degrade due to capacity fade and impedance increase that occurs during cycling. Monitoring capacity reduction and accurately predicting Remaining Useful Life (RUL) through battery management systems have become crucial, as the performance degradation of lithium-ion batteries can end up with critical risks such as thermal runaway reactions [2, 3]. Predicting the necessary replacement time in advance is challenging, due to intra-cell factors including morphology, architecture, and composition, as well as inter-cell factors such as winding, connection, and assembly processes that contribute to Cell-to-Cell Variability (CtCV) [4, 5], along with differences in operating conditions for each device. The Prognostics and Health Management (PHM) system implements condition-based management by predicting the necessary replacement timing before failures occur, allowing for repairment only when it's necessary [6, 7]. It considers battery capacity degradation using various sensor data, such as voltage, current, and temperature. RUL prediction is one of the critical functions of the PHM system, which forecasts the remaining cycles where the battery can be used safely. Accurate RUL prediction contributes to optimizing battery replacement timing and prevents accidents caused by excessive charging or discharging.

RUL prediction methods using early cycling behavior can generally be classified into two approaches: model-based approach and data-driven approach [8, 9]. However, model-based approaches often encounter challenges. In practice, the irreversible capacity fade is caused by an interaction of mechanical (e.g., particle cracking) and chemical (e.g., electrolyte decomposition) factors, making it quite difficult to mathematically identify these degradation mechanisms. Additionally, there can be a knee point where performance degradation, which progresses slowly in the early stages, accelerates after a certain cycle. This nonlinearity of performance degradation also contributes to the difficulty of model-based approaches. Machine Learning (ML)-based approach is a promising alternative to overcome this challenge [10–12].

ML-based RUL prediction research typically employs time series algorithms, with changes observed for each charging/discharging cycle. Traditionally, Recurrent Neural Network (RNN) [13–15] and Long Short-Term Memory (LSTM) [16] have been used for such tasks: Liu et al. [17] propose an adaptive RNN that continuously updates the parameters of the network to improve the description performance of dynamic cycling behavior of the LIBs. Park et al. [18] conducted RUL forecasting using LSTM, but they struggle with learning long-term dependency [19]. To overcome this limitation, the attention algorithm was introduced, enabling predictions that consider a broader context rather than just neighboring time steps [20, 21]. Designed for natural language processing task and centered around the attention algorithm, Transformer architectures outperforms RNN and LSTM by taking a bird’s-eye view of time-series data to learn features of data, then trains in order of importance rather than sequential dependency [22]. Chen et al. [23] conducted a prediction of RUL by Transformer, successfully overcoming the long-term dependency hurdle of RNN and LSTM. Despite being a *game changer* in time series forecasting, the Transformer has encountered difficulties when applied to time series prediction. Specifically, its high complexity in space (i.e., memory) time and its performance are not significantly superior to conventional LSTM models.

An alternative, DLinear, was proposed to address these challenges [24]. DLinear uses two linear layers considering trend and seasonality, in contrast to the complex structure and extensive computation of Transformer. Unlike the Transformer, DLinear takes both trend and seasonality into account in time series data predictions. Furthermore, it provides explainability with its weights of linear layers, revealing parameter importance. For battery life, RUL typically follows a decreasing trend with occasional increases. While the Transformer struggles to learn this trend, DLinear captures both the decreasing and periodic increasing trends, outperforming LSTM and Transformer-based predictions in aspects of space complexity and time complexity.

The performance of ML-based RUL prediction such as DLinear is determined by the quantity and quality of data. Since battery cycling experiments require a significant budget in time and cost, there are practical difficulties in generating large-scale datasets. Therefore, it is important to identify features that significantly contribute to battery lifespan and achieve high prediction performance even with a small number of training cycles. However, because high-dimensional features can overfit the cycling behavior used for training, selecting key features is essential, and various feature

engineering studies have been conducted to predict battery lifespan: Fei et al. [25] extracted 42 features from a large-scale lithium iron phosphate (LFP) battery dataset [11] and identified a high-performance prediction model structure by applying various feature selection approaches such as wrapper and filter approaches and various prediction models. Hu et al. [26] proposed a fusion approach that combines the advantages of wrapper and filter approaches to select features that contribute to state-of-health prediction. Greenbank et al. [27] propose an automatic feature selection method using the Pearson Correlation Coefficient (PCC), a filter approach, to predict the knee point where battery life declines rapidly and input the End-of-Life (EoL) prediction. However, the most widely used filter approach has concerns that correlation ranking can only consider linear dependencies between features and output. Shapley Additive exPlanation (SHAP) [28], which has recently been used in sensitivity analysis, provides insight at the feature selection stage because it presents qualitative results as well as quantitative sensitivity [29, 30]. Additionally, in Ref. [31], SHAP value-assisted feature selection was found to have superior performance compared to other algorithms for time series applications such as battery lifespan prediction. Moreover, the SHAP-based approach, which is a model-agnostic approach, is useful when applied to various machine learning models. In this study, we identify features that contribute to RUL prediction through the filter approach and SHAP-based approach and apply them to a ML model.

Here, we identify the features that contribute to the battery lifespan and predict the RUL of the battery using the DLinear model. Features contributing to battery capacity degradation were extracted based on battery chemistry. For the entire feature set, each key feature subset identified through the filter approach and SHAP-based approach is used as input for LSTM, Transformer, and DLinear, and the accuracy and EoL cycle are compared. The rest of this paper is structured as follows. In Section 2, the three machine learning algorithms used for the prediction of RUL are described. In Section 3, the dataset used in the cycling experiment and the scheme for extracting features contributing to the battery lifespan based on battery chemistry are explained. Additionally, two algorithms used for feature selection are introduced. Section 4 discusses feature engineering and RUL prediction results, and Section 5 presents a summary of the results and future work.

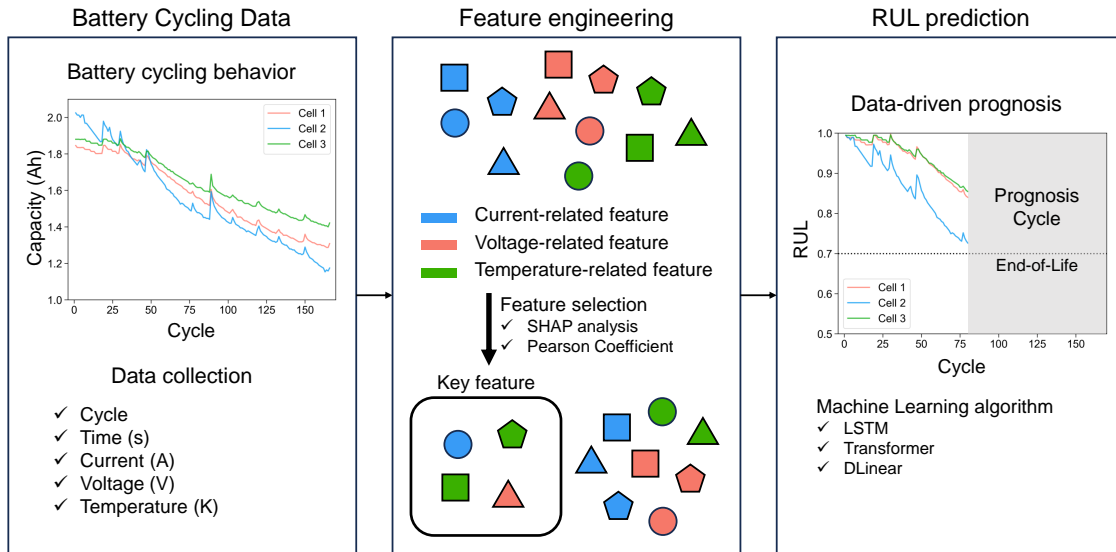


Figure 1: Schematic diagram of RUL prediction through feature engineering

## 2 Time-series prediction model

### 2.1 Long short-term memory (LSTM)

Sequential Neural Network (SNN) process time-series data by assuming that the state at any given time step depends on prior time steps. RNN is the pioneering SNN structure designed for processing time-series data [13–15]. The RNN model takes input to produce output, and also sends its output back to itself, to recurrent into the next time step. Due to this structure, each neuron in RNN has two sets of weights: one for input and another for multiplying with the output from the previous time step. In this way, RNN takes previous information into account and determines the extent of this reference with weights. However, it has pointed that as time progresses, the continuous multiplication of weights in RNN results in the dilution of information from distant past time steps at the current time step, a problem known as gradient vanishing [32].

To address this issue, the SNN known as LSTM was suggested, which divides the output from the previous time step into long-term state and short-term state. LSTM forwards them to the subsequent time steps. By introducing long-term state with minimal loss according to weights, LSTM improves the gradient vanishing problem observed in RNN.

## 2.2 Transformer

For a long time, LSTM has been firmly established as the state-of-the-art approach in time series data. However, long-term state of LSTM also did not completely solve the gradient vanishing problem [19]. The problem was alleviated but similar, as the consideration of information from distant past time steps being diluted as weights were multiplied with the long-term state of LSTM with the progression of time steps. Over time, an Attention algorithm was devised to focus more on contextually significant information after receiving information, not only from the immediate previous time step but from all time steps [20, 21]. This allowed for learning based on meaningful information from the entire dataset rather than focusing solely on nearby information, thereby addressing the issues of RNN, LSTM, and similar SNN algorithms. Furthermore, implemented with the Attention algorithm, the Transformer was devised. Recently, Transformer-based approaches and variant models of Transformer were utilized in predicting the RUL of LIBs [23].

## 2.3 DLinear

The Transformer has successfully overcome the hurdle of gradient vanishing and long-range dependencies posed by LSTM. However, as the Transformer was designed for natural language processing tasks (e.g., translation, summarization), not for time-series data, it had the weakness of poor performance when applied to time-series data. In particular, early Transformer models had difficulty in identifying trends in data that increased or decreased continuously throughout the observation period. Furthermore, due to its complex structure for analyzing sentences and texts written in languages, the Transformer required excessive computation compared to the conventional SNNs, thereby demanding a significant amount of time and memory. To address these two issues, DLinear was proposed [24].

The detailed procedure for RUL prediction using DLinear is introduced in *Algorithm 1*. DLinear separates time-series data into Trend ( $X_t$ ) and Remainder ( $X_s$ ) using a moving average, and learns each through a separate linear layer. Equation of  $X_t$  and  $X_s$  can be defined as follows:

$$X_t = \frac{1}{n} \sum_{k=0}^{n-1} X_{i-k} \quad (1)$$

---

**Algorithm 1** Decomposition-Linear (DLinear) Model for RUL Prediction

---

```
1: Input: Feature matrix  $X : [F_1, F_2, \dots, F_{20}]$ , Target  $y = \text{RUL}$ 
2: Step 1: Compute the moving average  $X_t$  using a sliding window
3: Step 2: Decompose into trend ( $X_t$ ) and remainder ( $X_s$ ) with  $X_s = X - X_t$ 
4: Step 3: Pass  $X_t$  and  $X_s$  through linear layers
5: if individual is True then
6:   for each feature  $i$  in  $X$  do
7:     Apply linear layers to predict future trend and seasonal components
8:   end for
9: else
10:  Use shared linear layers for all features
11: end if
12: Step 4: Combine predicted  $X_t$  and  $X_s$  to get final prediction
13: Output: Predicted time series data
```

---

$$X_s = X - X_t \quad (2)$$

where  $i$  is the time step of data, and  $n$  is the window size of the moving average. Based on the learning of these two linear layers, the future Trend and Remainder are predicted, and these two predictions are combined to derive the final prediction.

### 3 Feature engineering

In this section, feature engineering to extract parameters contributing to RUL from cycling data of LIBs and identify key parameters is explained. Our RUL prediction framework is validated using the NASA dataset [33]. In Section 3.1, the process of extracting features expected to contribute to lifespan through information on voltage, temperature, and time for four LIBs cells (i.e., B0005, B0006, B0007, and B0018) is described. In Section 3.2, the process by which a significantly contributing subset of the entire feature set is selected through the filter approach and SHAP-based approach is explained.

### 3.1 Feature extraction

In feature extraction, factors that contribute to RUL prediction are extracted based on battery cycling data collected from the Battery Management System (BMS). According to battery chemistry, the main factors that accelerate degradation are voltage [34] and temperature [35] during cycling, and degradation causes differences in charge and discharge profiles. Table 1 describes 20 features categorized by current and voltage, temperature, and time. Fig. 2(a-c) shows that the current and voltage profile at the charging stage, temperature distribution, and discharge voltage curve are dependent on the RUL. These dependent characteristics are processed through statistical information such as skewness and included in the feature set. In particular, the characteristic of the discharge curve, where differences occur after significant cycles, is explained by the slope at the early stage of the discharge (Fig. 2(d)).

Table 1: Description of features extracted for each parameter

Related parameter	Feature designation	Description
Current and Voltage	F <sub>1</sub>	Variance of measured voltage in discharging
	F <sub>2</sub>	Variance of measured current in discharging
	F <sub>3</sub>	Median of loaded voltage in discharging
	F <sub>4</sub>	Skewness of measured voltage in discharging
	F <sub>5</sub>	Skewness of loaded voltage in discharging
	F <sub>6</sub>	Slope of discharge voltage curve (50s to 500s)
	F <sub>7</sub>	Slope of discharge voltage curve (50s to 1000s)
	F <sub>8</sub>	Slope of discharge voltage curve (50s to 1500s)
Temperature	F <sub>9</sub>	Maximum temperature in discharging
	F <sub>10</sub>	Average temperature in discharging
	F <sub>11</sub>	Variance of temperature in discharging
	F <sub>12</sub>	Skewness of temperature in discharging
	F <sub>13</sub>	Minimum temperature in discharging
	F <sub>14</sub>	Maximum temperature in charging
	F <sub>15</sub>	Minimum temperature in charging
	F <sub>16</sub>	Average temperature in charging
Time	F <sub>17</sub>	Skewness of temperature in charging
	F <sub>18</sub>	CC charging time
	F <sub>19</sub>	CV charging time
	F <sub>20</sub>	Total discharging time

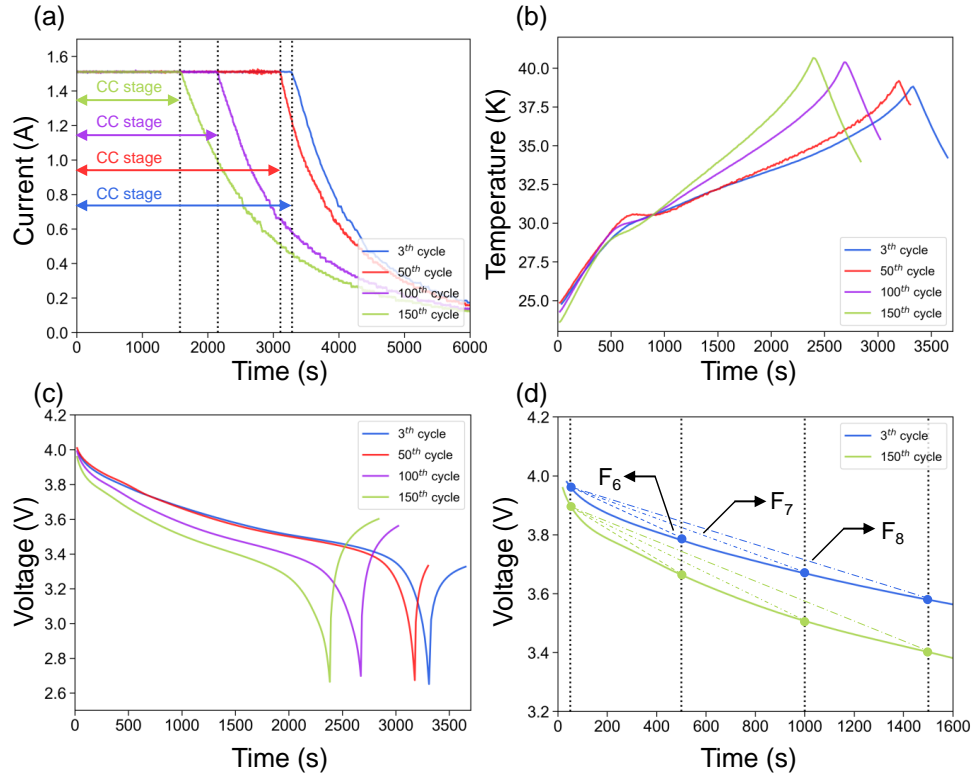


Figure 2: Feature description of charging and discharging for B0005 battery cell: (a) CC charging time ( $F_{18}$ ), (b) Temperature in discharging, (c) Voltage in discharging, (d): Slope of discharge voltage curve ( $F_6$ ,  $F_7$ , and  $F_8$ )

## 3.2 Feature selection

### 3.2.1 Filter approach

The filter approach uses feature ranking to select key features. In general, the correlation between the extracted features and the objective function (i.e., RUL) scores the ranking of each feature, selects features that are higher than a certain threshold, and screens other features [36]. Because the filter approach is applied without being integrated into the prediction model, it can be easily

applied to high-dimensional feature sets with relatively low computational budgets. This quantifies the linear correlation between the feature denoted by  $x$  and the objective function denoted by  $y$ .

$$r_{xy} = \frac{\sum_{i=1}^n (x_i - \bar{x})(y_i - \bar{y})}{\sqrt{\sum_{i=1}^n (x_i - \bar{x})^2 \sum_{i=1}^n (y_i - \bar{y})^2}}. \quad (3)$$

Where  $\bar{x}$  and  $\bar{y}$  are sample mean of  $x$  and  $y$ , respectively. As for the key feature selection, all correlation coefficients between key features and cell capacity are evaluated based on Eq. 3. The three parameter subsets with the highest absolute correlation coefficients are regarded as the *most sensitive features*, while those with the lowest absolute values are considered the *least sensitive features*. This concept also applies to the SHAP-based approach described in Section 3.2.2

### 3.2.2 SHAP-based approach

SHAP is an approach derived from Shapley values to explain the contribution of each feature to the predictions of a machine learning model. Originating from game theory, Shapley values aim to fairly distribute the contribution when players collectively achieve a specific outcome. Owen et al. [29] identified the relationship between Shapley values and variance-based global sensitivity analysis. The sum of the Shapley values for all features used in training a machine learning model is exactly equal to the total variance. This normalization property is quite crucial when determining the importance ranking of features. Sobol' indices, widely used in global sensitivity analysis, provide contributions for individual features similarly to SHAP, but when dependencies exist between features, the sum of sensitivities may not match the total variance [37]. In contrast, Shapley values work well even in the presence of dependencies between features. The Shapley value for feature  $F_i$  of a machine learning model is as follows:

$$\phi_i = \sum_{S \subseteq N \setminus \{i\}} \frac{|S|!(|N| - |S| - 1)!}{|N|!} [f(S \cup \{i\}) - f(S)]. \quad (4)$$

Where  $\phi_i$  is the Shapley value of the  $i$ -th feature  $F_i$ ,  $N$  is the set of all features (e.g., in our case,  $|N|$  is 20, see the Table 1),  $N \setminus \{i\}$  is the set of all possible combinations of remaining features excluding feature  $F_i$ ,  $S$  is a subset of  $N \setminus \{i\}$ ,  $f(S \cup \{i\})$  is the model prediction of the union of  $F_i$  and feature set  $S$ , and  $f(S)$  is the model prediction for the features in  $S$ .

# 4 Results and discussion

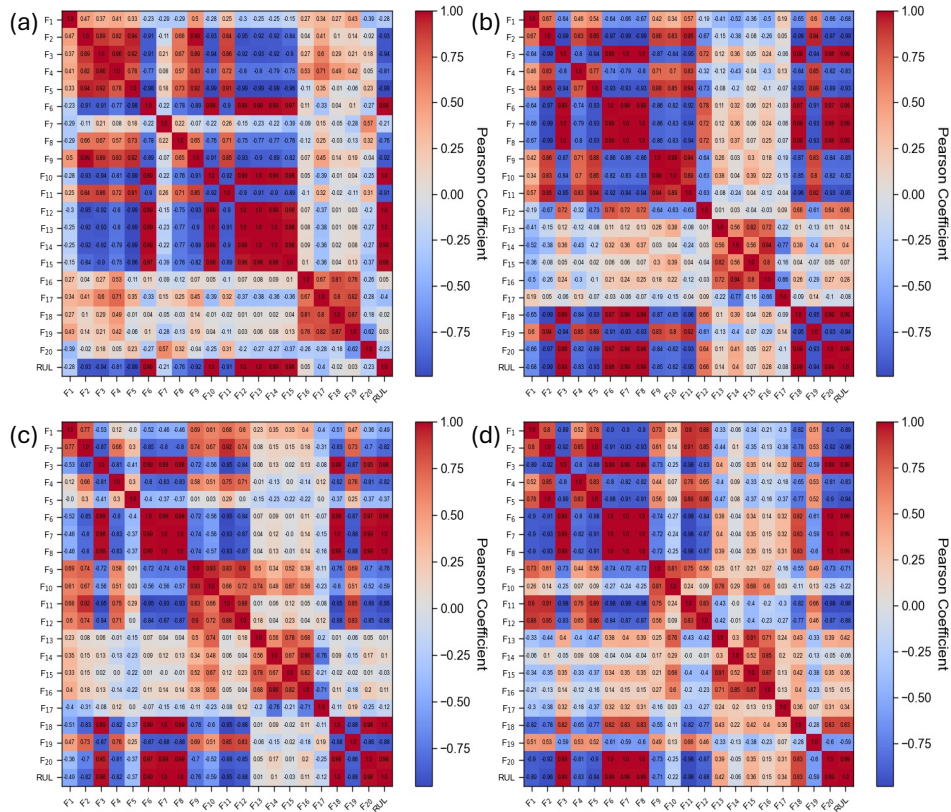


Figure 3: PCC of all parameters and RUL for four battery cells: (a) B0005 cell, (b) B0006 cell, (c) B0007 cell, (d) B0018 cell

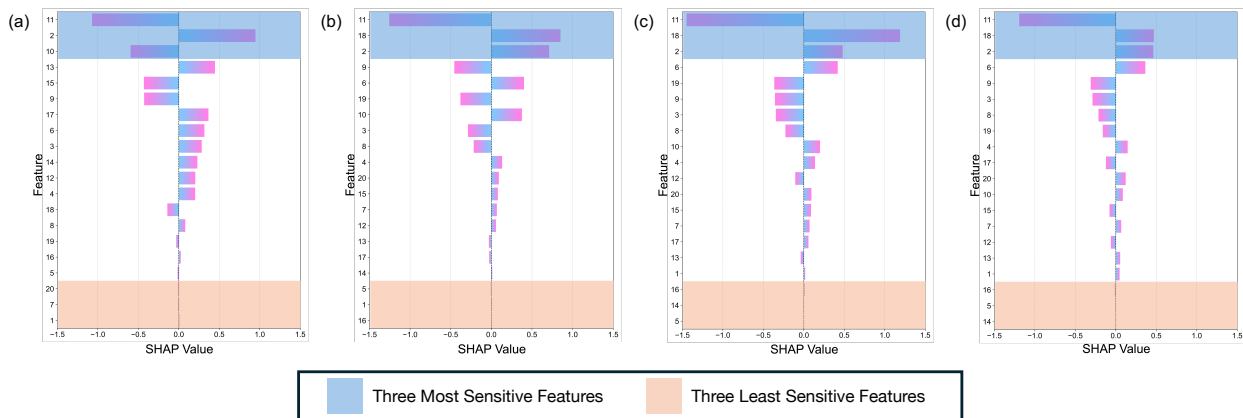


Figure 4: SHAP score of all parameters and RUL for four battery cells: (a) B0005 cell, (b) B0006 cell, (c) B0007 cell, (d) B0018 cell

The current, voltage, temperature, and time data collected from the cycling experiment were

reproduced into 20 features as shown in Table 1. Fig. 3 presents the results of PCC on 20 features for four cells. The three most sensitive features for each cell, as identified by the PCC, are:

- B0005:  $F_{10}$  (Average temperature in discharging),  $F_{12}$  (Skewness of temperature in discharging),  $F_{13}$  (Minimum temperature in discharging)
- B0006:  $F_3$  (Median of loaded voltage in discharging),  $F_{18}$  (CC charging time),  $F_{20}$  (Total discharging time)
- B0007:  $F_7$  (Slope of discharge voltage curve, 50s to 500s),  $F_8$  (Slope of discharge voltage curve, 50s to 1000s),  $F_{18}$  (CC charging time)
- B0018:  $F_7$  (Slope of discharge voltage curve, 50s to 500s),  $F_8$  (Slope of discharge voltage curve, 50s to 1000s),  $F_{20}$  (Total discharging time)

B0006, B0007, and B0018 include voltage characteristics during the discharging stage and time-related parameters during the charging or discharging stages as key parameters. In contrast, all three key parameters for B0005 are related to temperature characteristics, demonstrating significant variability across the four cells.

Fig. 4 shows the results of SHAP analysis, that  $F_2$  (Variance of measured voltage in discharging) and  $F_{11}$  (Variance of temperature in discharging) were selected as the highest values across all four cells. In addition to  $F_2$  and  $F_{11}$ ,  $F_{10}$  (Average temperature in discharging) was identified as one of the three most sensitive feature for B0005. Meanwhile,  $F_{18}$  (CC charging time), along with  $F_2$  and  $F_{11}$ , was identified as one of the three most sensitive feature for B0006, B0007, and B0018.

When training with the existing 70 cycles, the EoL prediction gap was well captured in Fig. 5. EoL was defined as 80% of the nominal capacity. In the case of LSTM, it captured and tracked the decreasing trend well after the training cycles. However, as the prediction progressed toward the later stages, it failed to follow the downward trend, resulting in a flat graph. This is because of the *gradient vanishing* problem mentioned previously.

The performance of Transformer was found to be inferior than LSTM due to the issue of *overstationarization*, which is considered a drawback of the Transformer algorithm [38]. Since the Transformer was originally developed for natural language processing rather than time-series data, it fails

to capture critical temporal dependencies in non-stationary time-series data with clear downward trends. Despite the fact that forecasting non-stationary time-series data is crucial for real-world applications including battery RUL predictions, such over-stationarization limits the prediction capability of the Transformer in these non-stationary time-series data. Previous studies on RUL prediction using Transformers [23, 39] have demonstrated that Transformers outperform LSTM in terms of predictive performance with revised model of Transformer. However, this study focuses on a comprehensive analysis of feature engineering considering CtCV and the improvement in RUL prediction performance driven by the characteristics of the DLinear algorithm. In this context, optimization of the model architecture was not considered in this study.

While LSTM and Transformer show a significant decrease in prediction performance as the training period decreases, DLinear maintained relatively accurate EoL prediction performance. Even when the training cycles were reduced to a maximum of 30 cycles, The performance of DLinear was observed to decline. Thus, DLinear demonstrated excellent performance in battery RUL prediction by separating the trend and seasonality of time-series data and learning them linearly, thereby effectively overcoming both the gradient vanishing problem of LSTM and the over-stationarization problem of the Transformer.

$$R^2 = 1 - \frac{SS_{\text{res}}}{SS_{\text{tot}}} \quad (5)$$

Fig. 6 illustrates the  $R^2$  scores of the models based on each algorithm, while Table 2 presents the MSE values according to the algorithm and the size of the training cycles, and Table 3 shows the corresponding  $R^2$  scores. The  $R^2$  score is not affected by the scale of the data, therefore particularly useful for evaluating battery data with varying training cycle lengths and total cycle durations. In contrast, MSE, by squaring the errors, sensitively captures large errors in time-series data and is differentiable, making it a commonly used loss function in machine learning algorithms. When evaluated using MSE and  $R^2$  score, DLinear’s performance was outstanding. The bolded values in Table 2 and Table 3 indicate the superior RUL prediction performance of DLinear. Even when the training cycles were reduced to 40, DLinear achieved an  $R^2$  score of 0.995.  $SS_{\text{res}}$  is the sum of squared differences between the observed values and the predicted values, and  $SS_{\text{tot}}$  is the sum of

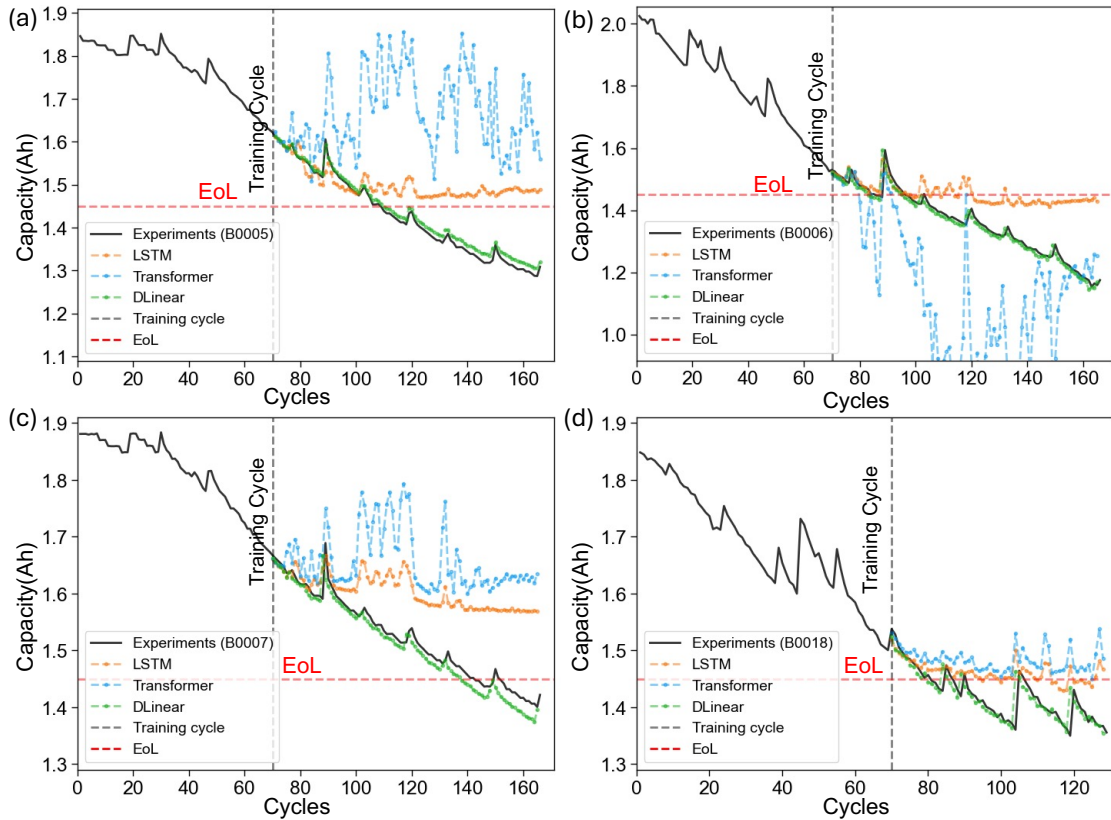


Figure 5: RUL prediction of four LIBs : (a) B0005, (b) B0006, (c) B0007, (d): B0018

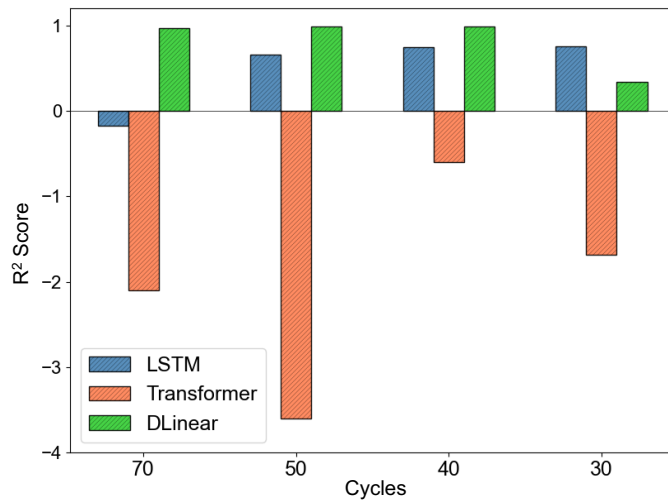


Figure 6: Comparison of  $R^2$  score according to algorithm and training cycle

squared differences between the observed values and the mean of the observed data. In cases where the model performs worse than simply predicting the mean of the observed values, the  $R^2$  score will be negative. This is because Eq. 5 subtracts the ratio of the residual sum of squares from 1,

meaning the resulting negative value is not constrained within the range of -1 to 1.

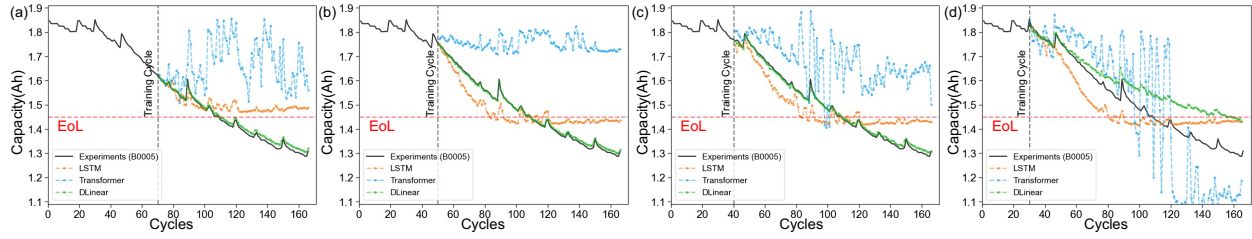


Figure 7: RUL prediction of B0005 according to training cycle : (a) 70 cycle, (b) 50 cycle, (c) 40 cycle, (d): 30 cycle

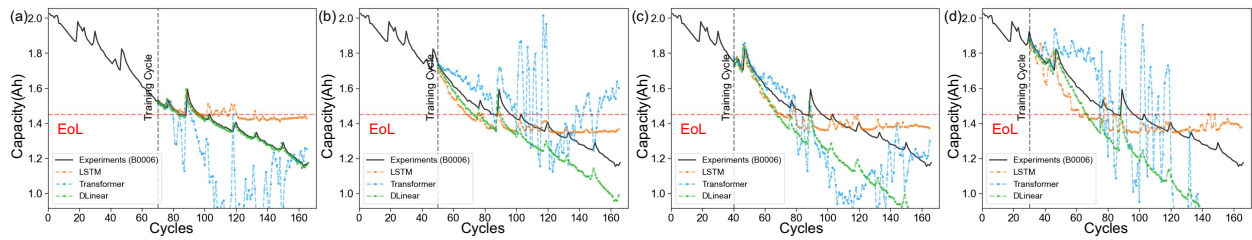


Figure 8: RUL prediction of B0006 according to training cycle : (a) 70 cycle, (b) 50 cycle, (c) 40 cycle, (d): 30 cycle

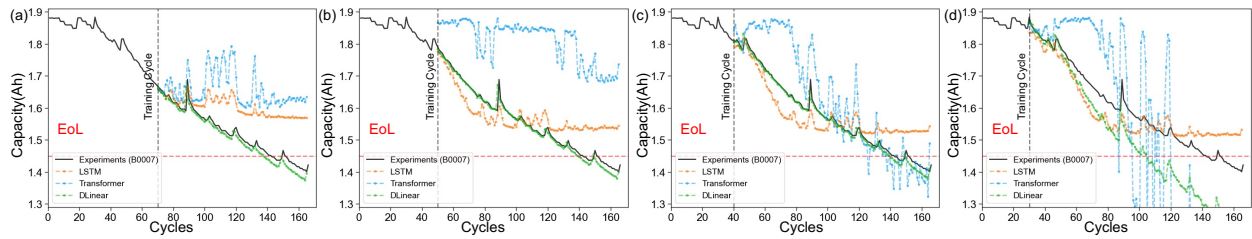


Figure 9: RUL prediction of B0007 according to training cycle : (a) 70 cycle, (b) 50 cycle, (c) 40 cycle, (d): 30 cycle

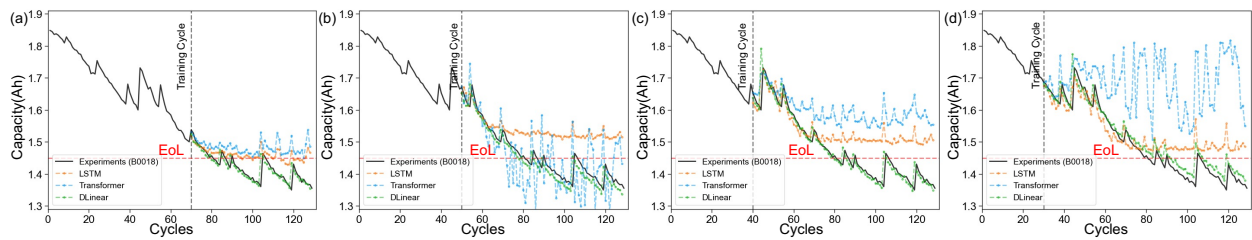


Figure 10: RUL prediction of B0018 according to training cycle : (a) 70 cycle, (b) 50 cycle, (c) 40 cycle, (d): 30 cycle

Table 2: Comparison of MSE by algorithm according to training cycle

Algorithm		Training Cycle			
		70	50	40	30
B0005	LSTM	0.03407	0.01821	0.01738	0.01999
	Transformer	0.15731	0.31750	0.11027	0.37554
	DLinear	<b>0.00003</b>	<b>0.00009</b>	<b>0.00019</b>	<b>0.00042</b>
B0006	LSTM	0.02038	0.00924	0.01089	0.01532
	Transformer	0.03699	0.24336	0.60980	0.35563
	DLinear	<b>0.00003</b>	<b>0.00006</b>	<b>0.00009</b>	<b>0.00019</b>
B0007	LSTM	0.04070	0.01757	0.01530	0.01355
	Transformer	0.02553	0.19942	0.10073	0.15515
	DLinear	<b>0.00007</b>	<b>0.00031</b>	<b>0.00062</b>	<b>0.00220</b>
B0018	LSTM	0.01101	0.03776	0.02583	0.01577
	Transformer	0.02165	0.02092	0.07549	0.20434
	DLinear	<b>0.00002</b>	<b>0.00003</b>	<b>0.00003</b>	<b>0.00006</b>

Table 3: Comparison of  $R^2$  by algorithm according to training cycle

Algorithm		Training Cycle			
		70	50	40	30
B0005	LSTM	-0.17398	0.66193	0.74823	0.75999
	Transformer	-2.10452	-3.59821	-0.59773	-1.68900
	DLinear	<b>0.98387</b>	<b>0.99705</b>	<b>0.99628</b>	0.68536
B0006	LSTM	-0.37580	0.63463	0.69113	0.66219
	Transformer	-1.49730	8.62568	16.29935	6.84430
	DLinear	<b>0.99772</b>	<b>0.34021</b>	-0.73222	-0.96263
B0007	LSTM	-0.69123	0.61148	0.74657	0.81998
	Transformer	-0.06079	3.40917	-0.66853	1.06123
	DLinear	<b>0.97061</b>	<b>0.99422</b>	<b>0.99511</b>	0.33864
B0018	LSTM	-0.57772	-0.40026	0.38087	0.67313
	Transformer	-2.10273	0.22419	-0.80949	3.21659
	DLinear	<b>0.99418</b>	<b>0.98418</b>	<b>0.99464</b>	0.95958

In PHM technologies, the ultimate goal is to achieve accurate predictions with fewer training cycles as possible. To evaluate whether this study can contribute to PHM technology, we progressively reduced the training cycles to 70, 50, 40, and 30 and analyzed the prediction performance. Fig. 7, 8, 9 and, 10 present the prediction results for four different battery cells (B0005, B0006, B0007, and B0018, respectively) while the number of training cycles was reduced. The corresponding MSE and  $R^2$  values are shown in Table 2 and Table 3. Reducing training cycles, LSTM exhibited poor performance, with its predictions deviating significantly from the actual values in the later stages, as shown in Fig. 5. Similarly, due to the over-stationarization issue, predictions made using the Transformer also demonstrated severe fluctuations which was to minimize the loss function, consistent with the behavior observed in Fig. 5. On the other hand, except for B0006 cell (Fig. 8), DLinear demonstrates superior prediction performance compared to LSTM and Transformer even

at 50 cycles and 40 cycles. However, except for B0018 (Fig. 10), there is a considerable difference between the real cycling behavior and the predicted cycling behavior when the training cycles are set to 30. In fact, recent research using Transformer demonstrates superior predictive performance compared to LSTM [23, 40]. However, this study focuses on feature engineering, and by using a simple network without considering improvements to the machine learning algorithms or hyperparameter tuning, it makes it easier to reproduce the results or apply this framework to other battery systems.

SHAP and PCC were employed for feature selection. Although using the three most sensitive features of performance of PCC resulted in higher prediction performance, there was a lack of consistency across different batteries (B0005, B0006, B0007, B0018, respectively). In contrast, while the three most sensitive features identified using SHAP yielded slightly lower prediction performance than the performance of PCC, they demonstrated consistency in feature selection across different batteries. This result suggests that SHAP-based feature selection has a higher potential for transfer learning between batteries, suggesting a certain level of robustness. In battery capacity research, sampling is often conducted to ensure representativeness that accounts for differences between cells, underscoring the importance of generalization performance. The consistent selection of the same features across multiple batteries indicates that these features are likely useful in a general context rather than being specific to individual cells. This consistency also implies potential reductions in future data collection and analysis costs, making it significant for broader applications.

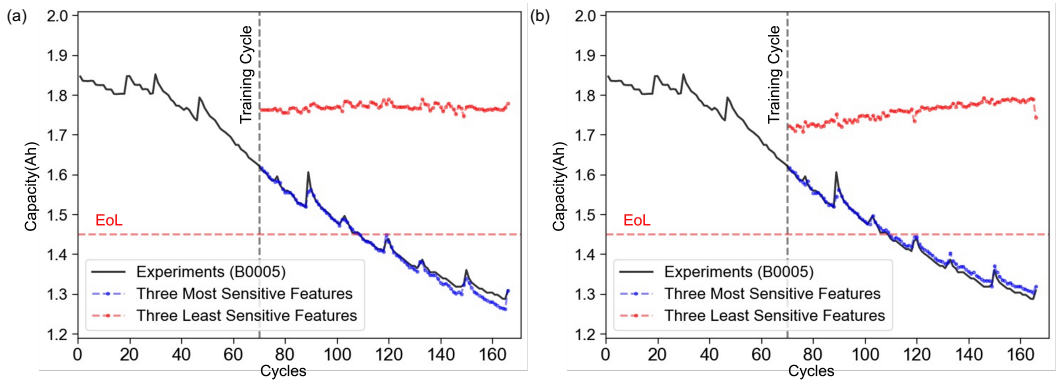


Figure 11: RUL prediction of B0005 cell according to feature selection: (a) PCC, (b) SHAP

Fig. 11 show the prediction results for B0005 cell using the sets of the three most sensitive fea-

Table 4: The most sensitive and least sensitive features in terms of importance, as determined by SHAP analysis

	B0005	B0006	B0007	B0018
Three most sensitive	2 <sup>a,*</sup> , 10, 11 <sup>a</sup>	2 <sup>a</sup> , 11 <sup>a</sup> , 18 <sup>a</sup>	2 <sup>a</sup> , 11 <sup>a</sup> , 18 <sup>a</sup>	2 <sup>a</sup> , 11 <sup>a</sup> , 18 <sup>a</sup>
Three least sensitive	1, 7, 20	1, 5 <sup>b</sup> , 14 <sup>b</sup>	5 <sup>b</sup> , 14 <sup>b</sup> , 16	5 <sup>b</sup> , 14 <sup>b</sup> , 16

\* Based on the feature selection results using SHAP, the extracted features, denoted by superscript <sup>a</sup>, are identified as key features in three or more cells, while those, denoted by superscript <sup>b</sup>, are identified as not significant in three or more cells.

Table 5: The three most sensitive and three least sensitive features in terms of importance, as determined by PCC

	B0005	B0006	B0007	B0018
Three most sensitive	10, 13, 12	18, 20, 3	7, 8, 18	7, 8, 20
Three least sensitive	17, 19, 20	13, 17, 15	13, 14, 15	10, 14, 16

tures and the three least sensitive features, as analyzed through PCC and SHAP, respectively. The sets of the three most sensitive parameters and the three least sensitive parameters, as determined by SHAP and PCC analyses, are presented in Table 4 and Table 5.

SHAP analysis reveals that more than half of the three most sensitive features are shared among batteries. A noteworthy point is, the key features identified by PCC differ significantly across the four cells, whereas those identified by SHAP analysis are identical for B0006, B0007, and B0018, with B0005 sharing two features with the other cells. A possible interpretation of these results is that the key parameters identified through SHAP-based sensitivity analysis provide robust results concerning CtCV. In practice, the uncertainties propagated by various causes, such as differences in electrode thickness during manufacturing stages (e.g., Calendaring process), imply that cycling behavior can vary even when cycling the same battery system under identical conditions [5]. The high robustness of SHAP suggests that it is a promising approach for predicting the RUL of large-capacity batteries (e.g., EVs) used in modules or packs.

Meanwhile, as shown in Table 5, PCC revealed cases where a feature ranked low for one battery was ranked high for another. For example,  $F_{10}$ ,  $F_{13}$ , and  $F_{20}$  were selected as the three most sensitive features based on PCC for some batteries, while they were in the three least sensitive features for others. These three features are related to temperature and time, and since batteries are significantly influenced by their surroundings, especially the ambient temperature, measurements such as maximum or minimum values can be affected by external factors or measurement errors. Therefore, these features appear to lack consistency in their significance across different batteries

when evaluated based on PCC.

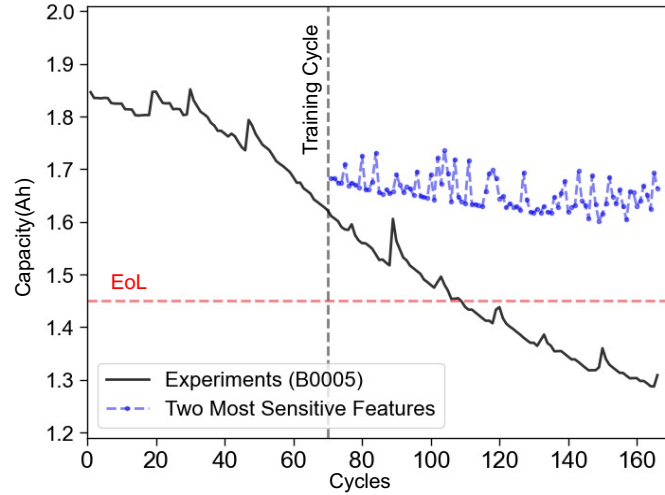


Figure 12: RUL prediction of B0005 cell using two most sensitive features identified by SHAP:  $F_2$ ,  $F_{11}$

In Table 4,  $F_2$  and  $F_{11}$  were consistently selected as the three most sensitive features across all four batteries. Building on this observation, we also examined the performance of predictions using only these two features. However, the performance did not match that of predictions made using three features. This suggests that, in addition to  $F_2$  and  $F_{11}$ , including additional features such as  $F_{18}$ , which encapsulate lifespan-related information, is recommended for improved prediction accuracy.

## 5 Conclusion

PHM technology involves real-time diagnosis and prediction of the health state of a target system. Accurate RUL prediction helps implement condition-based management, where interventions are taken only when necessary by predicting the preemptive system replacement point before failures or defects occur. However, predicting failures through RUL requires measuring charge/discharge data during real usage, which is impractical and time-consuming during experiments. Therefore, it's crucial to predict with higher accuracy using fewer experiments. In cases of clear trend-based predictions like battery degradation, DLinear outperforms models utilizing other algorithms. Even when trained on the same number of cycles, DLinear can predict further and more accurately than conventional LSTM or Transformer models. This suggests its potential contribution to implementing Condition Based Management for battery PHM technology in real industrial applications. On the other hand, identifying key features for predicting RUL aids in the implementation of PHM technology. PCC yields good performance for individual cells, but the key features vary significantly due to CtCV. Additionally, SHAP does not perform as well as PCC in terms of overall performance. However, SHAP consistently identifies key features, making it advantageous for battery research requiring generalization, despite the CtCV. Particularly, CtCV arises from both intra-cell factors such as morphology, architecture, and composition, and inter-cell factors like winding, connection, and assembly processes. Therefore, creating homogeneous batteries is challenging. In this regard, it is noteworthy that SHAP evaluates the importance of the same features despite CtCV.

## Code Availability

The code used in this work will be available after publication.

## References

- [1] B. Dunn, H. Kamath, and J.-M. Tarascon, *Science* **334**, 928 (2011).
- [2] D. P. Finegan, E. Darcy, M. Keyser, B. Tjaden, T. M. M. Heenan, R. Jervis, J. J. Bailey, R. Malik, N. T. Vo, O. V. Magdysyuk, R. Atwood, M. Drakopoulos, M. DiMichiel, A. Rack, G. Hinds, D. J. L. Brett, and P. R. Shearing, *Energy Environ. Sci.* **10**, 1377 (2017).
- [3] B. Mao, H. Chen, Z. Cui, T. Wu, and Q. Wang, *International Journal of Heat and Mass Transfer* **122**, 1103 (2018).
- [4] M. Kim and J. Kim, *ACS Sustainable Chemistry & Engineering* **12**, 6786 (2024).
- [5] M. Kim, J. Schaeffer, M. D. Berliner, B. P. Sagnier, M. Z. Bazant, R. Findeisen, and R. D. Braatz, *Journal of The Electrochemical Society* **171**, 090517 (2024).
- [6] K. Goebel, B. Saha, A. Saxena, J. R. Celaya, and J. P. Christophersen, *IEEE Instrumentation & Measurement Magazine* **11**, 33 (2008).
- [7] D. Beck, P. Dechent, M. Junker, D. U. Sauer, and M. Dubarry, *Energies* **14** (2021), 10.3390/en14113276.
- [8] G. Prasad and C. Rahn, *Journal of Power Sources* **232**, 79 (2013).
- [9] J. He, Z. Wei, X. Bian, and F. Yan, *IEEE Transactions on Transportation Electrification* **6**, 417 (2020).
- [10] B. Zhou, C. Cheng, G. Ma, and Y. Zhang, *IOP Conference Series: Materials Science and Engineering* **895**, 012006 (2020).
- [11] K. A. Severson, P. M. Attia, N. Jin, N. Perkins, B. Jiang, Z. Yang, M. H. Chen, M. Aykol, P. K. Herring, D. Fraggedakis, *et al.*, *Nature Energy* **4**, 383 (2019).
- [12] S. Ai, J. Song, and G. Cai, *Mathematics* **10** (2022), 10.3390/math10101733.
- [13] J. J. Hopfield, *Proceedings of the National Academy of Sciences* **79**, 2554 (1982), <https://www.pnas.org/doi/pdf/10.1073/pnas.79.8.2554> .

- [14] D. E. Rumelhart, G. E. Hinton, and R. J. Williams, “Learning internal representations by error propagation,” in *Parallel Distributed Processing: Explorations in the Microstructure of Cognition, Vol. 1: Foundations* (MIT Press, Cambridge, MA, USA, 1986) p. 318–362.
- [15] M. Jordan, *Serial order: a parallel distributed processing approach. technical report, june 1985-march 1986*, Tech. Rep. (California Univ., San Diego, La Jolla (USA). Inst. for Cognitive Science, 1986).
- [16] S. Hochreiter and J. Schmidhuber, *Neural Computation* **9**, 1735 (1997).
- [17] J. Liu, A. Saxena, K. Goebel, B. Saha, and W. Wang, in *Annual Conference of the PHM Society*, Vol. 2 (2010).
- [18] K. Park, Y. Choi, W. J. Choi, H.-Y. Ryu, and H. Kim, *IEEE Access* **8**, 20786 (2020).
- [19] Y. Bengio, P. Simard, and P. Frasconi, *IEEE Transactions on Neural Networks* **5**, 157 (1994).
- [20] D. Bahdanau, K. Cho, and Y. Bengio, “Neural machine translation by jointly learning to align and translate,” (2016), arXiv:1409.0473 [cs.CL] .
- [21] M. Luong, H. Pham, and C. D. Manning, *CoRR* **abs/1508.04025** (2015), 1508.04025 .
- [22] A. Vaswani, N. Shazeer, N. Parmar, J. Uszkoreit, L. Jones, A. N. Gomez, L. Kaiser, and I. Polosukhin, *CoRR* **abs/1706.03762** (2017), 1706.03762 .
- [23] D. Chen, W. Hong, and X. Zhou, *Ieee Access* **10**, 19621 (2022).
- [24] A. Zeng, M. Chen, L. Zhang, and Q. Xu, *Proceedings of the AAAI Conference on Artificial Intelligence* **37**, 11121 (2023).
- [25] Z. Fei, F. Yang, K.-L. Tsui, L. Li, and Z. Zhang, *Energy* **225**, 120205 (2021).
- [26] X. Hu, Y. Che, X. Lin, and S. Onori, *IEEE Transactions on Transportation Electrification* **7**, 382 (2020).
- [27] S. Greenbank and D. Howey, *IEEE Transactions on Industrial Informatics* **18**, 2965 (2021).

- [28] S. M. Lundberg and S.-I. Lee, *Advances in neural information processing systems* **30** (2017).
- [29] A. B. Owen, *SIAM/ASA Journal on Uncertainty Quantification* **2**, 245 (2014).
- [30] B. Vuillod, M. Montemurro, E. Panettieri, and L. Hallo, *Reliability Engineering & System Safety* **234**, 109177 (2023).
- [31] Y. Gebreyesus, D. Dalton, S. Nixon, D. De Chiara, and M. Chinnici, *Future Internet* **15**, 88 (2023).
- [32] Y. Bengio, P. Simard, and P. Frasconi, *IEEE transactions on neural networks / a publication of the IEEE Neural Networks Council* **5**, 157 (1994).
- [33] N. O. D. Portal, “Li-ion battery aging datasets,” .
- [34] R. Klein, N. A. Chaturvedi, J. Christensen, J. Ahmed, R. Findeisen, and A. Kojic, *Proceedings of the 2011 american Control Conference*, , 382 (2011).
- [35] F. Leng, C. M. Tan, and M. Pecht, *Scientific reports* **5**, 12967 (2015).
- [36] P. Sedgwick, *BMJ* **345** (2012).
- [37] Z. Li, *Computers, Environment and Urban Systems* **96**, 101845 (2022).
- [38] Y. Liu, H. Wu, J. Wang, and M. Long, (2023), arXiv:2205.14415 [cs.LG] .
- [39] Z. Zhang, W. Song, and Q. Li, *IEEE Transactions on Instrumentation and Measurement* **71**, 1 (2022).
- [40] W. Gomez, F.-K. Wang, and J.-H. Chou, *Energy* **296**, 131114 (2024).